Soft Matter

Dynamic Article Links

Cite this: *Soft Matter*, 2011, **7**, 9051

www.rsc.org/softmatter

PAPER

Self-similarity in electrorheological behavior

Manish Kaushal and Yogesh M. Joshi*

Received 5th May 2011, Accepted 22nd June 2011
DOI: 10.1039/c1sm05825h

In this work we study the creep flow behavior of a suspension of polyaniline (PANI) particles in silicone oil under the application of an electric field. A suspension of PANI in silicone oil, a model electrorheological (ER) fluid, shows an increase in the elastic modulus and the yield stress with an increase in the magnitude of the electric field. Under the creep flow field, the application of a greater magnitude of electric field reduces the strain induced in the material while application of a greater magnitude of shear stress at any electric field enhances the strain induced in the material. Remarkably, the time evolution of strain in a PANI suspension at different stresses, electric field strengths and concentrations show superposition after appropriate shifting of the creep curves on the time and strain axes. Observed *electric field–shear stress–creep time–concentration superposition* demonstrates self-similarity in electrorheological behavior. We analyze the experimental data using the Bingham and Klingenberg–Zukoski models and observe that the latter predicts the experimental behavior very well. We conclude by discussing the remarkable similarities between the observed rheological behavior of ER fluids and the rheological behavior of aging soft glassy materials.

I Introduction

Electric field induced polarization of colloidal particles suspended in low conducting organic media is known to cause a rapid increase in the yield stress and viscosity of the suspension.[1–3] These changes, first reported by Winslow,[4] are known as electrorheological phenomena. Over the decades electrorheological behavior has been extensively studied both experimentally and theoretically by various groups.[1–3,5–15] Recent efforts in this field are focused on understanding the mechanisms of the ER effect and developing new materials that show more enhanced behavior. Recently a renewed interest has developed in this subject among researchers due to the observation of a very large electrorheological effect where an increase in the yield stress of the order of 100 kPa is reported,[16,17] which is significantly larger than that observed for conventional ER fluids ($\leq$1kPa).[1] Due to the electrically induced increase in rigidity and yield stress along with the reversibility associated with this phenomenon, ER fluids find potential applications in clutches, shock absorbers, activators, *etc.*

The electrorheological (ER) fluid usually consists of electrically polarizable particles having a diameter in the range of 1 to 100 μm suspended in a hydrophobic liquid.[1] The effectiveness of an ER fluid depends on the extent of mismatch between the polarizability (or conductivity) of the colloidal particles and that of the liquid in which particles are suspended. Electric field induced polarization of the particles eventually causes the formation of a chain like structure in the direction of electric field. The formation of chains that span the gap between electrodes, resists any movement of the electrodes that tends to stretch them. The net enhancement of rigidity of an ER fluid therefore depends on the force of attraction among the particles forming the chain and number of chains per unit area. The volume fraction and size distribution of the suspended particles determine the number of chains per unit area and the arrangement of particles within the chains. Under the application of a shear deformation field, the chains stretch. When tension in the chains overcomes the attractive forces among the particles, chains rupture causing yielding.[1,4,9] According to the point–dipole approximation of the polarization model, in which effect of surrounding particles is ignored in estimating the dipole moment of a particle, the force of attraction between two particles is estimated to be proportional to the square of a product of electric field strength and relative polarizability (β^2E^2).[9] Relative polarizability is given by $\beta = (\varepsilon_p - \varepsilon_s)/(\varepsilon_p + 2\varepsilon_s)$, where ε_p and ε_s are the polarizabilities of the colloidal particles and that of the liquid respectively. For an ER fluid, the yield stress for an idealized situation where single particle width chains span the gap has been estimated to be proportional to: $\sigma_y \sim \phi\beta^2E^2$,[9] where ϕ is the volume fraction of the monodispersed particles and E is the mean field strength. The polarization model works well for low electric field strength or for high frequency AC fields.[18] For a DC field or for a low frequency AC field, the charges migrate to the particle and screen out the dipoles.[1] Under such conditions the mismatch in the conductivities of the particle and that of the suspending medium dominates the ER effect wherein relative polarizability is given by $\beta = (\sigma_p - \sigma_s)/(\sigma_p + 2\sigma_s)$,[1] where σ_p and σ_s are the conductivities of the colloidal

Department of Chemical Engineering, Indian Institute of Technology Kanpur, Kanpur, 208016, India. E-mail: joshi@iitk.ac.in

particles and that of the liquid respectively. According to the conduction model the yield stress dependence on the electric field is given by, $\sigma_y \propto \sqrt{E_c}E^{1.5}$ where E_c is the critical field strength above which conductivity effects dominate.[19,20] Therefore, the power law exponent of the yield stress dependence on the electric field (obtained from experiments) gives an idea about the underlying mechanism of the ER effect.

The very fact that the ER fluid does not flow unless yield stress is overcome makes this system suitable for the application of the Bingham plastic model, wherein shear stress in excess of yield stress is directly proportional shear rate and is given by: $\sigma_{12} - \sigma_y = \eta_{pl}\dot{\gamma}$, where $\dot{\gamma}$ is shear rate and σ_{12} is shear stress.[21] The constant of proportionality is called plastic viscosity (η_{pl}) and is considered to be the suspension viscosity without the applied electric field.[9] In the literature, other constitutive relations that employ the concept of yield stress but are different from the Bingham model have also been proposed to support experimental observations.[22] Overall the electric field tends to form a chain like structure while the imposed flow field tends to fluidize the particles. The relative importance of polarization forces to that of hydrodynamic forces is expressed by the Mason number and is given by: $Ma = \eta_s\dot{\gamma}/2\varepsilon_0\varepsilon_s\beta^2E^2$, where η_s is the viscosity of the solvent and ε_0 is the permittivity of space. The greater the Mason number is, the greater is the effect of hydrodynamic forces.

Klingenberg and Zukoski[9] studied the steady state flow behavior of an electrorheological fluid consisting of hollow silica spheres in corn oil. They observed that under a constant shear rate, the suspension in the shear cell bifurcates into coexisting regions containing fluidized particles and a solid region formed by the tilted broken chains. Both the fluid and solid regions were observed to be in the plane of velocity and vorticity, perpendicular to the direction of electric field. They also proposed a model by considering the concentration gradient in the shear cell in the direction of electric field. Under steady shear, consideration of coexisting solid–fluid regions showed good agreement with the experimental behavior. Contrary to observation of coexisting solid–fluid regions, many groups reported the appearance of a lamellar structure in steady shear flow. The surface normal of lamella or stripes was observed to be oriented in the vorticity direction.[23–26] Recently Von Pfeil *et al.*[27,28] proposed a two fluid theory by developing a continuum model by accounting for the hydrodynamic and electrostatic contributions to net particle flux. The model predicted the formation of stripes in a sheared suspension below a critical Mason number. On the other hand, above a critical Mason number, the dominance of the hydrodynamic contribution produced a uniform concentration profile. Although both the flow profiles, namely fluid–solid coexistence and stripe formation, are observed experimentally, it is not clear what the specific conditions are that are responsible for each of them.

Interestingly various rheological features of ER fluids demonstrate great similarity to those observed for soft glassy materials.[29] Soft glassy materials are those soft materials that are thermodynamically out of equilibrium. Common examples are concentrated suspensions and emulsions, foams, cosmetic and pharmaceutical pastes, *etc.* Apart from the observation of yield stress in both of these apparently dissimilar systems, namely ER fluids and soft glassy materials, there are two very striking similarities between them. The first one is an effect of the strength of the electric field on ER fluids to that of the effect of aging time on soft glassy materials. Both these variables tend to increase the yield stress and rigidity of the respective materials. The second likeness is the effect of the stress or deformation field. In both ER fluids as well as soft glassy materials, the application of a deformation field tends to destroy or break the structure responsible for enhancement of rigidity.[30,31] Interestingly ER fluids are also observed to show viscosity bifurcation[32] similar to that observed for soft glassy materials;[33] wherein depending upon the value of applied stress, the viscosity of a flowing fluid bifurcates either to a very large value stopping the flow or remains small allowing the continuation of the flow as a function of time. In soft glassy materials the rheological response to a step strain or step stress (creep) is different for experiments carried out at different aging times and under different deformation fields. This is due to a change in material properties caused by these two variables. However, the appropriate rescaling of process time (time elapsed since application of step strain or step stress) with respect to aging time and the stress (deformation) field has been observed to collapse all the data to form universal master curves leading to *process time–aging time–stress superposition.*[30,31,34,35] Considering the similarity of the rheological behavior of ER fluids and soft glassy materials, we believe that it is possible to observe process time–electric field–stress correspondence in the former system as well. In this work we have explored the electrorheological behavior of a polyaniline (PANI)–silicone oil ER fluid in a creep flow field at different electric field strengths, shear stresses and concentrations. Interestingly, we do observe creep time–electric field–stress–concentration superposition and other similarities in flow behavior of ER fluids and soft glassy materials.

II Material and experimental procedure

The ER fluid composed of polyaniline (PANI) particles suspended in silicone oil has been investigated by many groups due to its thermal and chemical stability.[36,37] The low density of polyaniline (sp. gravity = 1.33) reduces the rate of sedimentation while the high dielectric constant and low conductivity help, providing an enhanced electrorheological effect.[37] In this work we synthesize polyaniline *via* oxidative polymerization as suggested in the literature.[38] Polymerization was carried out using an equimolar solution of aniline hydrochloride and ammonium peroxodisulfate (oxidant). As the reaction is exothermic, a dropwise reaction was carried out to avoid a sudden temperature rise by pouring the oxidant solution drop by drop into the aniline hydrochloride solution. During this process, the reaction mixture, whose temperature is maintained at 2–5 °C, was stirred gently using a magnetic stirrer. Following the stirring, the reaction mixture was left for 24 h at 0 °C. Subsequently it was filtered and washed with ethanol to remove excess reactants and to make the particle surface hydrophobic.[39] Finally drying is carried out to obtain greenish polyaniline hydrochloride. In this reaction HCl protonates PANI thereby enhancing the electric conductivity of the same, causing a reduction in ER effect. Therefore, the precipitated PANI was washed with ammonia solution which lowers the conductivity and makes the ER effect more pronounced. The PANI precipitate was dried for 24 h at 80 °C,

and then the dried PANI was ground using a mortar and pestle to reduce it into powder form. The particle size of the PANI powder was analyzed using two methods, scanning electron microscope and dynamic light scattering. Fig. 1 shows a SEM image of the PANI powder. The particle size analysis estimated the mean diameter to be around 1.5 μm with a polydispersity index (P.I.) of 0.636. Dried PANI powder was mixed with silicon oil using manual mixing followed by sonication for 5 min. In this work we have used four concentrations of PANI in the range 5–15 weight %. The silicon oil used in this work is Newtonian with a shear viscosity of 0.36 Pa s and has a sp. gravity of 0.97.

In this work, we have used an Anton Paar, Physica MCR 501 rheometer with an electrorheological accessory. We have employed a parallel plate geometry with diameter 25 mm. In this work, we carried out oscillatory shear and creep experiments. The strength of the electric field was varied in the range of 0 to 12 kV mm^{-1} by applying DC voltage across two parallel plates 0.5 mm apart. In all the experiments the deformation field was applied after applying the electric field. All the experiments were carried out at 25 °C.

III. Results

In order to evaluate the effectiveness of the electrorheological phenomena, it is necessary to measure the magnitude of the elastic (storage) modulus and the yield stress and their dependence on the strength of the electric field. Fig. 2 shows the results of oscillatory experiments as a function of the strength of the electric field (E). The inset of Fig. 2 shows the time dependent evolution of the elastic modulus (G') after applying the electric field to the PANI suspension for the oscillatory experiments carried out for a 5 Pa magnitude of shear stress at a frequency of 0.1 Hz. It can be seen that the elastic modulus increases as a function of time and eventually reaches a plateau. Furthermore, with the increase in the strength of the electric field, the time required for the elastic modulus to attain a plateau decreases. The process of the evolution of the elastic modulus is associated with the polarization of the particles and their subsequent movement to form a chain like structure. As expected, the timescale associated with polarization and that of the movement decreases with the electric field. A similar phenomenon was also reported for electrically activated clay nanocomposites system wherein Park and coworkers[40] reported superposition of modulus evolution curves obtained at different electric fields. In Fig. 2, a plateau value of the elastic modulus is plotted as a function of the strength of the electric field. It can be seen that the elastic modulus shows a power law dependence on the electric field given by: $G' \propto E^{1.33}$. For a monodispersed ER suspension of spherical particles that form a chain having a one particle width, point–dipole approximation predicts quadratic dependence of the elastic modulus on the electric field.[41] The present system, which is far from an idealized situation of point–dipole limit, shows weaker dependence on the electric field. Such deviation may also arise from other factors such as polydispersity and conductivity effects.

Having analyzed PANI–silicone oil ER fluid for elastic modulus, we turn to creep experiments. Fig. 3 shows the creep flow behavior of a 5 weight % suspension at a constant stress of 100 Pa for varying strengths of electric field. It can be seen that the suspension undergoes a lesser deformation with an increase in the strength of the electric field. Eventually at a sufficiently

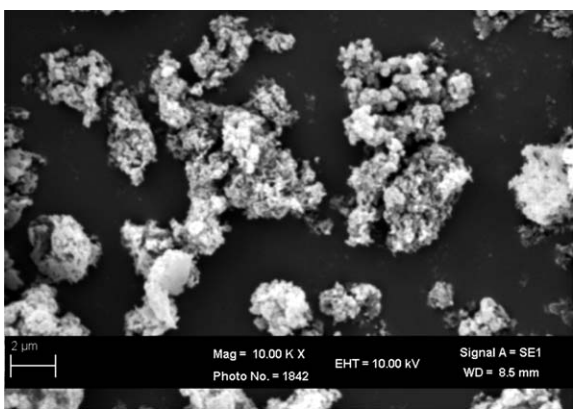

Fig. 1 Scanning electron microscope image of polyaniline powder. Particle size analysis gives the mean diameter to be around 1.5 μm.

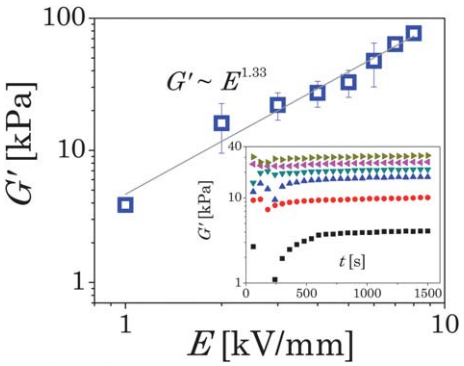

Fig. 2 Behavior of elastic modulus as a function of electric field for 5 wt.% PANI suspension. Inset shows evolution of elastic modulus as a function of time after the electric field has been applied (from top to bottom: 6, 5, 4, 3, 2, 1 kV mm^{-1}). It can be seen that elastic modulus attains a constant value beyond 600 s. In the main plot elastic modulus is observed to demonstrate a power law dependence on electric field strength given by: $G' \propto E^{1.33}$.

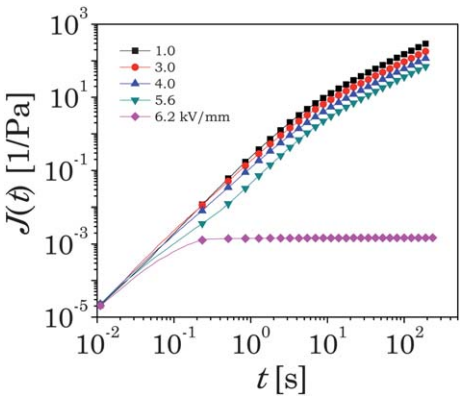

Fig. 3 Creep compliance is plotted against creep time at various electric field strengths for a constant stress of 100 Pa for a 5 wt.% PANI suspension. At greater electric field strengths compliance shows a weaker increase, eventually showing a plateau at a very high electric field.

high electric field, compliance reaches a plateau and the suspension stops flowing. In Fig. 4, the time evolution of compliance in a fixed electric field is plotted for different shear stresses for a 5 weight % suspension. It can be seen that compliance decreases with a decrease in the magnitude of the shear stress and that, below the yield stress of a suspension, flow stops and compliance attains a plateau. Fig. 3 and 4 suggest that there is a similarity between the creep behavior of the ER suspension with respect to an increase in electric field strength or a decrease in stress. Moreover the creep curves in both the figures have a similar curvature.

In a creep experiment the minimum stress at which a material starts flowing is known as the yield stress of the material associated with an applied electric field strength. In Fig. 5, we have plotted the yield stress of a 5 weight % PANI suspension computed using creep experiments as a function of the electric field. It can be seen that yield stress shows a power law dependence with exponent 0.86. We also carried out an oscillatory stress sweep experiment to estimate the yield stress of the material at various electric fields, which leads to: $\sigma_y \propto E_0^{1.4}$. Theoretically the yield stress is proposed to have a quadratic dependence on the electric field according to the polarization model,[9] whereas according to the conduction model the yield stress dependence on the electric field is given by $\sigma_y \propto E_0^{1.5}$. Since the focus of this paper is on creep behavior and self similarity associated with the same, we use the estimation obtained from the creep test in the analysis of the data.

Recently, a lot of work has been carried out to understand the creep behavior of soft glassy materials that undergo physical aging as a function of time elapsed since the jamming transition. Aging in soft glassy materials involves an increase in the elastic modulus and the yield stress as a function of time. Consequently, creep experiments carried out at greater aging times induce lesser strain in the material.[34] Soft glassy materials also undergo partial shear melting or rejuvenation under the application of the deformation field, which reduces the elastic modulus of the material.[42] Therefore, application of shear stress having greater magnitude induces greater compliance in the material. Overall an increase in the elastic modulus and the yield stress shown in Fig. 2 and 5 and evolution of compliance as observed in Fig. 3 and 4 shows similar trends when the strength of the electric field is replaced by aging time (time elapsed since the jamming transition

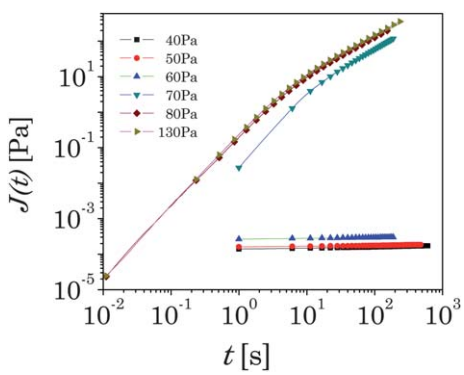

Fig. 4 Creep compliance is plotted against creep time for different stresses at constant electric field strength 4 kV mm^{-1} for a 5 wt. % PANI suspension.

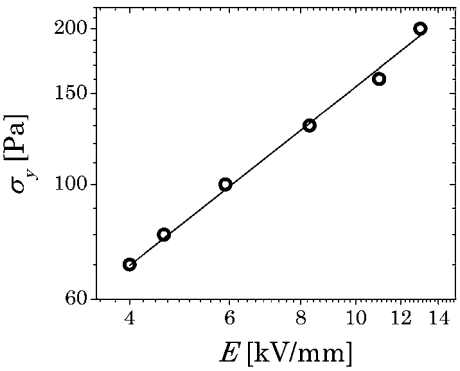

Fig. 5 Yield stress obtained from creep experiments is plotted with respect to electric field strength. The points show experimental data while the line shows a power law fit to the data: $\sigma_y = a' E_0^b$, with $a' = 0.052 \pm 0.02$ and $b = 0.86 \pm 0.043$.

in soft glassy materials). For example, Fig. 2 of the present paper which shows an increase in the elastic modulus as a function of the electric field is qualitatively similar to Fig. 1 of Bandyopadhyay *et al.*[43] where an increase in the elastic modulus is observed as a function of aging time. Similarly Fig. 5 of the present paper that depicts an increase in the yield stress with the electric field strength demonstrates the same trend as observed for a soft glassy material where an increase in the yield stress is observed as a function of aging time as shown in Fig. 5 of Negi and Osuji.[44] Furthermore, Fig. 3 of the present paper showing creep behavior at constant stress but with different electric fields is qualitatively similar to inset of Fig. 2 of Shahin and Joshi,[34] where experiments were carried out at constant stress and different aging times. Then again, Fig. 4 of the present paper that shows the creep behavior at a constant electric field but different stresses is qualitatively similar to Fig. 1 of Coussot *et al.*[45] in which creep stress is varied at constant aging time. In soft glassy materials, it is observed that the self-similar curvature of evolution of compliance as a function of aging time leads to demonstration of time–aging time superposition.[31,34,35] Moreover, horizontal shifting of time–aging time superpositions obtained at different creep stresses produces time–aging time–stress superposition.[30] Therefore, by the observed qualitative analogy between soft glassy materials and ER suspensions and due to the similar curvature observed for compliance in Fig. 3 and 4, electric field and stress dependent data suggest a possibility of superposition on the time axis.

In Fig. 6 we have plotted the horizontally shifted creep curves shown in Fig. 4 representing experiments carried out at stress of 100 Pa but with different electric field strengths. It can be seen that the creep curves superpose very well leading to a time–electric field superposition. Similar to the superposition shown in Fig. 6, the creep curves obtained at various other stresses (in the range 80 Pa to 200 Pa) also demonstrate excellent superpositions upon horizontal shifting. In Fig. 7 we have plotted the corresponding horizontal shift factors as a function of electric field that are associated with individual time–aging time superpositions obtained at different creep stresses. Fig. 7 shows that shift factors decrease with an increase in electric field strength. However, the decrease in shift factor can be seen to be becoming weaker with an increase in the magnitude of creep stress. In order

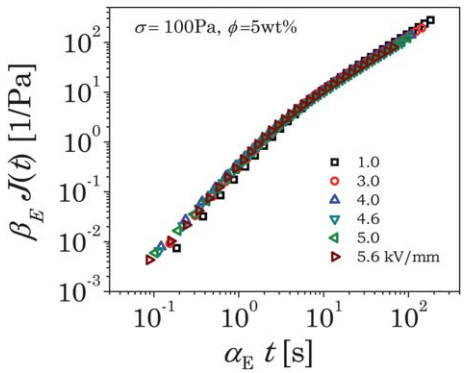

Fig. 6 Electric field–time superposition for a constant stress of 100 Pa for a 5 wt. % PANI suspension. All the creep curves at different electric field strengths (1–6 kV mm^{-1}) superpose to produce a master curve.

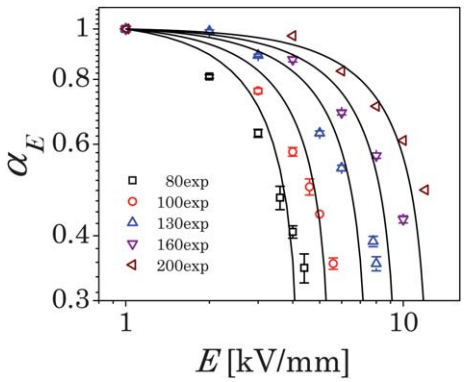

Fig. 7 Horizontal shift factors required to obtain an electric field–time superposition, at various creep stresses are plotted against electric field strengths. The line shows the fit of a modified Bingham model (eqn (3)).

to get the superposition, we also needed to apply a very minor vertical sifting (β_E in the range 1 to 1.2) to a few creep curves. In all the five superpositions obtained at constant stress, we have horizontally shifted various creep curves at higher electric fields to a creep curve at 1 kV mm^{-1}. Interestingly, for 5 weight % PANI suspension, at 1 kV mm^{-1} electric field strength, evolution of compliance with time is observed to be independent of stress ($\alpha_\sigma = 1$, $\beta_\sigma = 1$, for 1 kV mm^{-1} over the explored range of stresses). The horizontal shifting of all the creep curves obtained at different electric fields and stresses onto that of obtained at 1 kV mm^{-1}, therefore leads to a comprehensive superposition of all the creep curves associated with each point shown in Fig. 7. In Fig. 8 we have plotted time–electric field–stress superpositions of 30 creep curves obtained at different electric field strengths (1–12 kV mm^{-1}) and creep stresses (80–200 Pa) for a 5 weight % PANI ER suspension.

We also carried out creep experiments on ER fluids having different concentrations of PANI. In Fig. 9 we have plotted creep curves for four concentrations of PANI suspensions at creep stress of 100 Pa and electric field strength of 1 kV mm^{-1}. As expected, evolution of compliance shows weaker growth with an increase in the concentration of PANI. However, creep curves can be seen to be demonstrating similar curvature suggesting a possibility of the inclusion of concentration in the superposition as well. Fig. 10 demonstrates the "time–electric field–stress–concentration

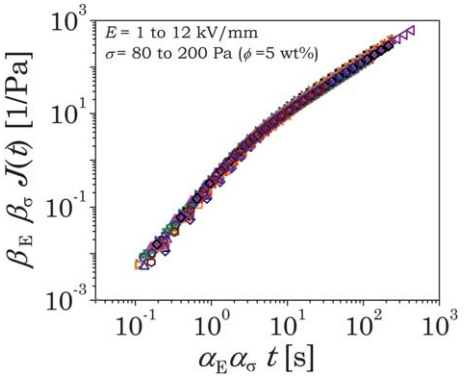

Fig. 8 Electric field–stress–time superposition for a 5 wt. % PANI suspension. This superposition includes 30 creep curves obtained at different electric fields in the range 1 to 12 kV mm^{-1} and different creep stresses in the range 80 to 200 Pa.

superposition" by horizontally and vertically shifting the concentration dependent curves shown in Fig. 9 on to superposition associated with a 5 wt. % concentration. In Fig. 10, we have plotted 49 creep curves obtained at different electric fields, stresses and concentrations. The corresponding concentration dependent horizontal and vertical shift factors have been plotted in Fig. 11. Concentration dependent horizontal shift factors are observed to decrease while that of vertical shift factors are observed to increase with an increase in concentration. Observation of time–electric field–stress–concentration superposition suggests that the creep behavior of an electrorheological fluid under smaller electric fields, lower concentrations and greater shear stresses over shorter duration is equivalent to long term creep behavior at higher electric fields, greater concentrations and smaller shear stresses.

IV. Discussion

Owing to the fact that ER fluids under an electric field demonstrate yield stress, traditionally their flow is modeled using a Bingham constitutive equation: $\sigma_{12} - \sigma_y = \eta_{pl}\dot{\gamma}$.[9] In the Bingham model, material flows only for stresses greater than the yield stress. Furthermore, under flow conditions, the rate of deformation (shear rate) is proportional to the shear stress in excess of the yield stress. In the present work, the Bingham model

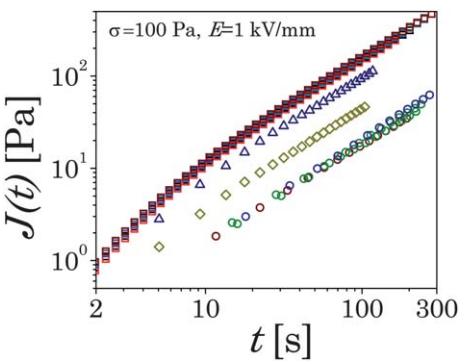

Fig. 9 Effect of concentration of PANI on the creep behavior (From top to bottom (in wt. %): 5, 10, 13, 15). PANI suspension shows lower compliance for a system having a higher concentration.

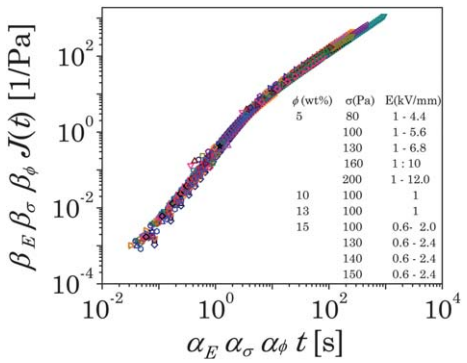

Fig. 10 Electric field–stress-concentration–time superposition. The master curve is obtained by superposing 49 creep curves for various stresses, electric filed strengths and concentrations as shown in the figure.

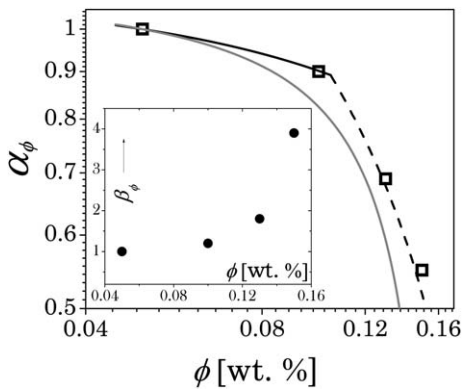

Fig. 11 Horizontal (α_ϕ) shift factors plotted as a function of concentration of PANI. The gray line is the fit of a modified Bingham model (eqn (11)) to the horizontal shift factor data. On the other hand, the fit of a K–Z model is represented by the solid black line (eqn (12)) and the dashed black line (eqn (13)) to the horizontal shift factor data. Dependence of the vertical shift factor (β_ϕ) on concentration is shown in an inset.

was observed to be inadequate to fit the shift factor behavior shown in Fig. 7. The inadequacy of the Bingham model to fit the rheological behavior of ER fluids has been reported earlier as well.[7,13] In order to impart greater flexibility to the Bingham model, we modified the same as:

$$\sigma_{12}^m - \sigma_y^m = (\eta_{pl}\dot{\gamma})^m, \tag{1}$$

where, exponent m adjusts an extent of influence of yield stress on the flow behavior of a material, with $m = 1$ giving the Bingham model while $m = 0.5$ leads to the Casson model.[21] For a creep flow, evolution of compliance can be obtained by integrating eqn (1) to give:

$$J = \frac{1}{\eta_{pl}}\left[1 - \left(\sigma_y/\sigma_{12}\right)^m\right]^{1/m} t + c' \tag{2}$$

where c' is a constant of integration. In Fig. 8, we shift the experimental creep data obtained at different electric field strengths and stresses on to data obtained at $E_0 = 1$ kV mm^{-1}, for which $\sigma_y/\sigma_{12} \ll 1$. This leads to horizontal shift factor for modified Bingham model to be:

$$\alpha = \frac{\left[1 - \left(\sigma_y/\sigma_{12}\right)^m\right]^{1/m}}{\left[1 - \left(\sigma_{y1}/\sigma_{12}\right)^m\right]^{1/m}} \tag{3}$$

where σ_{y1} is yield stress at 1 kV mm^{-1}.

We fit eqn (3) to the shift factor data shown in Fig. 7. We use the same expression for yield stress that was obtained by fitting a power law to the experimental data shown in Fig. 5. As shown in Fig. 7, eqn (3) demonstrates a reasonable fit to the data for $m = 2$. Increase in m beyond unity suggests that the effect of yield stress wanes off more rapidly at higher shear stresses and approaches a Newtonian limit earlier than that for Bingham model. It can be seen that the modified Bingham model indeed fits the experimental behavior qualitatively. However, curvatures of the model prediction in comparison with that of the experimental behavior leave a lot to be desired. This suggests that more physical insight is necessary to explain the experimental behavior than the empirical approach of a modified Bingham model.

As mentioned in the introduction section, upon application of an electric field, particles dispersed in the suspension undergo polarization which eventually leads to the formation of chains in the direction of the electric field. Application of a deformation field stretches these chains causing tilting of the same in the flow direction.[1,9,16] Klingenberg and Zukoski (K–Z)[9] proposed that the chains rupture beyond a critical tilt angle which results in yielding. In an ER fluid undergoing a constant shear rate, K–Z observed coexisting regions of solid and fluid. In addition, the fraction of the fluidized domain in the shear cell was observed to increase with the shear rate (refer to Fig. 5 to 8 of Klingenberg and Zukoski[9]). In order to model this behavior, K–Z assumed variation of concentration in the solid region in the direction of electric field. The concentration induced variation of yield stress produced coexisting solid and fluid regions over a range of shear stresses. The concentration variation proposed by K–Z showed decrease in concentration from wall to center and was symmetric and continuous at the center. They however claimed that the results of the model are insensitive to the details of the concentration profile. They further proposed a simple empirical relation between local yield stress σ_y, electric field strength E_0 and local concentration φ_l, given by: $\sigma_y = aE_0^b\varphi_l^r$, where a, b and r are constants. Therefore, for stresses below $\sigma_{y0} = aE_0^b\varphi_0^r$, where φ_0 is a concentration at the center, the solid phase fills the entire gap, while for stresses above $\sigma_{ym} = aE_0^b\varphi_m^r$, where φ_m is a concentration at the wall, fluid phase occupies the entire gap. For an intermediate region, there is a coexistence of fluid and solid regions. Overall the shear stress–shear rate relation proposed by K–Z is given by:[9]

$$\text{for } \sigma_{12} < \sigma_{y0},\ \dot{\gamma} = 0, \tag{4}$$

$$\text{for } \sigma_{y0} \le \sigma_{12} < \sigma_{ym},\quad \eta_\infty\dot{\gamma}/\sigma_{12} = \{[(\sigma_{12}/\sigma_{y0})^{1/r} - 1]/[(\varphi_m/\varphi_0) - 1]\}^{1/n}, \tag{5}$$

$$\text{for } \sigma_{12} \ge \sigma_{ym},\ \eta_\infty\dot{\gamma}/\sigma_{12} = 1, \tag{6}$$

where η_∞ is the viscosity of the fluid region considered to be independent of the electric field. The concentration at the center

(φ_0) and the exponent n are the parameters associated with the concentration profile such that φ_m gets fixed due to the mass balance for the overall volume fraction φ. Shear compliance can be estimated by integrating eqn (1) and (2) with respect to time to give:

$$\text{For } \sigma_{y0} \leq \sigma_{12} < \sigma_{ym},$$
$$J = (\{[(\sigma_{12}/\sigma_{y0})^{1/r} - 1]/[(\varphi_m/\varphi_0) - 1]\}^{1/n}/\eta_\infty)t + c_1 \quad (7)$$

$$\text{For } \sigma_{12} \geq \sigma_{ym},\ J = t/\eta_\infty + c_2, \quad (8)$$

where $c_1$and c_2 are constants of integration.

An analysis of Fig. 3 and 4 from the point of view of the above discussion suggests that the curves for which compliance shows a plateau belong to a solid phase occupying the complete gap and are described by eqn (4). The curves for which compliance is continuously increasing and is greater for greater shear stress or lower electric field belong to the states where fluid–solid regions coexist and are described by eqn (5) or (7). At high shear stresses, when the fluid region occupies the complete gap, the compliance curves are independent of the shear stress as well as the strength of electric field; eqn (6) or (8) describe the dynamics.

For a 5 weight % PANI suspension, at electric field strength of 1 kV mm^{-1}, the compliance curves do not show any dependence on shear stress. Therefore, according to the K–Z model, at 1 kV mm^{-1} the fluid phase completely occupies the shear cell for the explored shear stresses. In Fig. 6, we have shifted all the compliance curves associated with the higher electric fields and different shear stresses onto compliance curves belonging to 1 kV mm^{-1} electric field strength. Therefore, according to the K–Z model the horizontal shift factor required to obtain the superposition shown in Fig. 8 is given by:

$$\text{for } \sigma_{y0} \leq \sigma_{12} < \sigma_{ym},\ \alpha = \{[(\sigma_{12}/\sigma_{y0})^{1/r} - 1]/[(\varphi_m/\varphi_0) - 1]\}^{1/n} \quad (9)$$

$$\text{and for } \sigma_{12} \geq \sigma_{ym},\ \alpha = 1 \quad (10)$$

In Fig. 12 we have plotted the fit of eqn (9) and (10) to the experimental data. It can be seen that for an expression of yield stress obtained in Fig. 5, and for various model parameters $r = 2.2$, $n = 2.73$ and $\varphi_0 = 0.032$, $\varphi_m = 0.059$ (for 5 weight % PANI, $\varphi = 0.036$), eqn (9) and (10) show an excellent fit to the experimental data. A discontinuity in the curvature of eqn (9) and (10) apparent in Fig. 12 is due to the discontinuity in $\dot{\gamma}$ associated with eqn (5) and (6) at $\sigma_{12} = \sigma_{ym}$. Overall, the proposal of the K–Z model that the shear cell gets bifurcated into coexisting solid and fluid phases explains the observed phenomena very well.

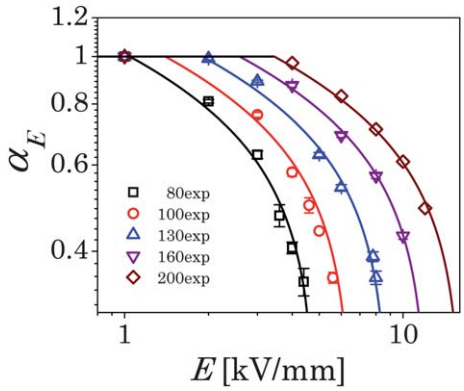

Fig. 12 Fit of a K–Z model to the horizontal shift factors shown in Fig. 7. Symbols show the experimental data while lines show fit to the K–Z model (eqn (9) and (10)).

It is important to note that the K–Z model considers that the fluid phase always obeys a Newtonian constitutive relation. Therefore, for $\sigma_{12} \geq \sigma_{y0}$ an increase in the stress or an increase in the fluid fraction tends to progressively lower the effect of the yield stress, and in the limit of $\sigma_{12} \geq \sigma_{ym}$ the flow behavior is completely independent of the yield stress. On the other hand, the flow of a Bingham fluid is always influenced by the yield stress. In the modified Bingham model represented by eqn (1), values of the exponent m greater than unity tend to reduce influence of the yield stress with an increase in the applied stress. Therefore, for experimental data where the value of α rapidly decreases towards unity over a short range of electric field strengths, it is not surprising that a modified Bingham model shows a qualitative fit to the experimental data for a value of m much greater than unity.

In order to obtain the electric field–stress–concentration–time superposition shown in Fig. 10, vertical shifting of the creep curves obtained at different concentrations is also needed along with the horizontal shifting. It can be seen that neither eqn (2) associated with a modified Bingham model, nor eqn (7) and (8) associated with the K–Z model account for any vertical shifting. We believe that the necessity of vertical shifting is due to transient response in the evolution of creep curves. It should be noted that the K–Z model represented by eqn (4)–(6) is associated with steady state fractions of coexisting fluid and solid phases of ER fluid. Integration of eqn (5) and (6) (eqn (7) and (8)), which represents a linear relationship between compliance and time, is therefore a steady state flow behavior. At small creep times, however, the system undergoes a transient response wherein momentum transfer from the moving wall to the stationary wall leads to the evolution of fluid–solid phases. Due to gradient of concentration prevailing in the ER fluid, momentum transport in systems having different concentrations can indeed expected to be different. Therefore, in order to predict the behavior of the vertical shift factors shown in Fig. 11, which are necessary to shift the concentration dependent creep curves shown in Fig. 9, the concentration dependent transient behaviour needs to be considered.

Fig. 11 also shows the behavior of the horizontal shift factor, which is seen to be decreasing with an increase in concentration of PANI. The concentration dependent horizontal shift factors can easily be determined for both the models. For a modified Bingham model the shift factor is given by:

$$\alpha = \frac{\left\{\eta_{pl,\varphi 1}\left[1 - \left(\sigma_{y,\varphi}/\sigma_{12}\right)^m\right]^{1/m}\right\}}{\left\{\eta_{pl,\varphi}\left[1 - \left(\sigma_{y,\varphi}/\sigma_{12}\right)^m\right]^{1/m}\right\}} \quad (11)$$

For the K–Z model the shift factor depends on the maximum and minimum concentrations in the concentration profile for a particular concentration and is given by:

for $\sigma_{y0,\varphi} \leq \sigma_{12} < \sigma_{ym,\varphi}$,

$$\alpha = \frac{\{\eta_\infty\}_{\varphi=\varphi_1}}{\{\eta_\infty\}_{\varphi}} \left\{ \left(\left[\left(\sigma_{12}/\sigma_{y0} \right)^{1/r} - 1 \right] \Big/ \left[\left(\varphi_m/\varphi_0 \right) - 1 \right] \right)^{1/n} \right\}_{\varphi} \quad (12)$$

and for

$$\sigma_{12} \geq \sigma_{ym,\varphi},\ \alpha = \frac{\{\eta_\infty\}_{\varphi=\varphi_1}}{\{\eta_\infty\}_{\varphi}} \quad (13)$$

where $\varphi_1 = 0.036$ (5 weight %) is the concentration of the reference creep curve on which all the other curves have been superposed, while $\sigma_{y0,\varphi}$ and $\sigma_{ym,\varphi}$ are respectively the maximum and minimum concentrations in the profile associated with concentration φ. Viscosity η_{pl} associated with the modified Bingham model and η_∞ associated with the K–Z model are dependent on the concentration of PANI in the suspension. In eqn (11)–(13) we use the Krieger–Dougherty equation for concentration dependence given by:[1]

$$\eta_{pl} = \eta_\infty = \eta_s \left(1 - \frac{\varphi}{\varphi_c} \right)^{-[\eta]\varphi_c} \quad (14)$$

where η_s is the solvent viscosity, φ_c is the volume fraction associated with close packing which we take to be 0.68 and $[\eta]$ is the intrinsic viscosity which we consider to be 2.5.[1] Finally we again consider the same expression of yield stress obtained in Fig. 5. Fig. 11 shows fits of eqn (11), (12) and (13) to the experimental data. It should be noted that other than φ_c and $[\eta]$, the same fitting parameters used in Fig. 7 and 12 lead to the fit shown in Fig. 11. Considering the polydispersity associated with the suspended particles, the high value of the random packing volume fraction φ_c is expected. It can be seen that the K–Z model fits the data very well, however the modified Bingham model does not give a good fit to the shift factor data for an assumed value of φ_c.

In the previous section, we discussed various similarities shared by the rheological behavior of the ER suspension and that of soft glassy materials. In soft glassy materials, due to physical jamming, the translational diffusivity of the constituents of the same is severely constrained so that material has access to a limited part of the phase space. Such a situation kinetically hinders the material from achieving thermodynamic equilibrium. Generically the various constituents of soft glasses are considered to be trapped in potential energy wells such that mere thermal energy is not sufficient to let the constituents jump out of the well. In such a situation these constituents undergo activated dynamics of structural rearrangement so as to attain progressively lower potential energy as a function of time.[46] The application of a deformation field increases the potential energy of the particle, and when this increase is of the order of the depth of the energy well the particle escapes out of the well and a local yielding event takes place. Application of a strong deformation field facilitates the escape of all the trapped particles from their respective wells causing the complete yielding of the material. Cloitre and coworkers[31] reported this phenomenon experimentally wherein they observed that below the critical stress σ_c, the deformation field is not strong enough to induce practically any local yielding, and aging is unaffected by the application of stress. However, above σ_c the deformation field induces local yielding events which lead to partial shear melting (or partial rejuvenation) of the soft glassy material. An increase in stress above σ_c progressively reduces the magnitude of the aging dynamics. Finally when stress exceeds yield stress σ_y of the material, complete shear melting takes place and the material stops aging. Analogous to soft glasses, the model of Klingenberg and Zukoski also proposes two stresses: σ_{y0} and σ_{ym}, the former one is associated with lowest concentration of polarized ER fluid in the shear cell while the latter stress is associated with the maximum concentration. When the stress exceeds σ_{y0}, the material flows; however there exists a fluid–solid coexistence until the stress σ_{ym} is overcome. Beyond σ_{ym} the effect of the electric field diminishes and the material flows like a Newtonian fluid. Remarkably this behavior is very similar to that observed in soft glasses.

Contrary to the observation of coexistent fluid and solid regions in the plane of velocity and vorticity, recently many groups have observed stripe or lamella formation in a plane of the electric field and velocity below a critical Mason number.[23–26] All the cases that report stripe formation were shear rate controlled and in many cases the electric field was imposed after the deformation field was applied. Von Pfeil and coworker's[27,28] two fluid model, wherein imposition of an electric field was considered on the suspension undergoing shear, predicted the observed behavior very well. Von Pfeil and coworker's proposal suggested that below a critical Mason number, where stripe formation is observed, the response of shear stress is expected to be dependent on time (transient), while above a critical Mason number, where the suspension shows a uniform concentration profile, the shear stress should remain constant.[23] It should be noted that our experiments are stress controlled and the stress field is imposed after applying the electric field. However, in order to check the transient behavior of our experiments, we plot the evolution of the shear rate as a function of time at various electric field strengths for a creep stress of 100 Pa in Fig. 13. It can be seen that all the creep curves overcome transient response in less than 10 s and show a steady state thereafter. In Fig. 14, we have plotted the slope of the shear rate curve ($\dot{\gamma}_{avg}$) averaged over a duration of 10 s to 200 s. It can be seen that, for all the explored electric fields, the slope of the shear rate–creep time curve is close to zero in the considered region. It has already been mentioned that for an electric field strength of 1 kV mm^{-1}, the evolution of

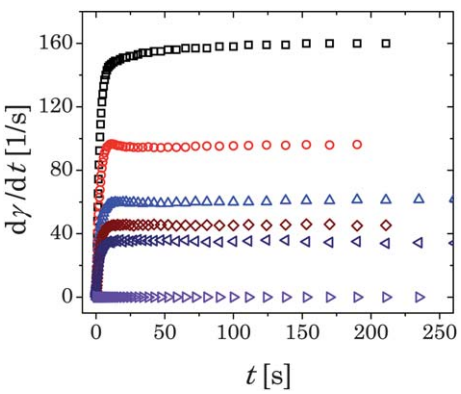

Fig. 13 Evolution of shear rates as a function of creep time for experiments carried out at 100 Pa and various electric field strengths for data shown in Fig. 3 (from top to bottom: 1, 3, 4, 5, 5.6 and 6.2 kV mm^{-1}).

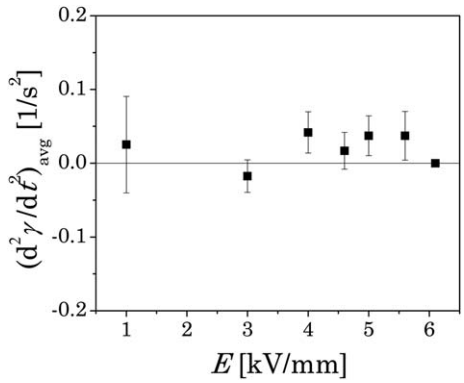

Fig. 14 Average of the time derivative of shear rates shown in Fig. 13 is plotted as a function of applied electric field strength for creep experiments carried out at 100 Pa. An average was estimated for the duration: 10 s to 200 s.

compliance is independent of the applied shear stress, suggesting the complete fluidization of the suspended particles. On the other hand at 6.2 kV mm^{-1}, the ER fluid does not flow for a 100 Pa creep stress. Fig. 3 (the compliance curves for the shear rate curves shown in Fig. 13) demonstrates a qualitatively similar evolution of strain in the span of 1 to 5.6 kV mm^{-1}, wherein flow undergoes a complete fluid to solid transformation. The observation of creep time–electric field–stress–concentration superposition also suggests that all the creep curves have a self-similar curvature and hence the evolution of shear rate has the same qualitative behavior as shown in Fig. 13. Therefore, the observed behavior in the present work, wherein the imposition of the electric field precedes the creep is not equivalent to the various recent observations of a transient response above a critical electric field wherein the shear rate was imposed prior to the electric field. Although the experimental behavior reported in the present paper is well explained by the Klingenberg and Zukoski model, direct visual observation is necessary to determine nature of the flow field, whether fluid–solid coexistence or stripe formation. Moreover, more work is necessary to clearly distinguish the conditions under which either of the flow fields is expected.

V Conclusion

In this paper we study the creep flow behavior of a model electrorheological fluid: PANI–silicone oil suspension having different concentrations under the application of varying electric field strengths and shear stresses. As a generic feature, under a constant electric field the suspension undergoes greater deformation at higher stress, while under constant stress the deformation induced is lesser for greater electric field strengths. Experiments carried out with increasing concentration of PANI in silicone oil, show lesser compliance. Nonetheless, beyond a yield point, irrespective of electric field, stress and concentration, the evolution of compliance as a function of time demonstrates similar curvatures shifted on time and compliance axes. Horizontal and vertical shifting of the compliance–time curve leads to time–electric field–stress–concentration superposition. The corresponding horizontal shift factors decrease with either an increase in the strength of the electric field, a decrease in the stress or with an increase in concentration.

We analyze the observed behavior of the shift factors using two models, namely: a modified Bingham model and the Klingenberg–Zukoski model. In the modified Bingham model, we consider that beyond the yield stress, an ER fluid follows a constitutive relation given by: $\sigma_{12}^m - \sigma_y^m = (\eta_{pl}\dot{\gamma})^m$, where the parameter m governs the effect of the yield stress on a flowing suspension. The fit of a modified Bingham model to the time and electric field dependent shift factor data leads to $m = 2$. This suggests that the effect of the yield stress diminishes with an increase in stress faster than that of the Bingham model. The theory of Klingenberg–Zukoski proposes that the gradient of the concentration induced in the polarized particles upon application of the electric field leads to a gradient of yield stress in the direction of the electric field. Therefore, constant shear stress induces coexistence of fluid and solid regions. The fluid zone, where yield stress is lower than the shear stress, is proposed to follow a Newtonian constitutive relation. We observe that the Klingenberg–Zukoski model gives an excellent prediction of the observed behavior of electric field, stress and concentration dependent shift factors.

Interestingly, various rheological observations reported in this work show a striking similarity with the rheological behavior of soft glassy materials when an electric field is replaced by aging time. These observations include: an increase in the elastic modulus and yield stress with the electric field, the evolution of compliance under the application of electric field and stress, and observation time–electric field–stress superposition. Moreover, the model of Klingenberg–Zukoski, which gives an excellent fit to the shift factor data, suggests the presence of two threshold stresses that are associated with yield stresses of maximum and minimum concentrations of the concentration profile within the shear cell. If the applied stress is in between these two limits, only a partial yielding of the electrorheological material takes place. Interestingly, such two shear stress limits, within which only partial yielding (or rejuvenation) takes place, have also been observed for soft glassy materials.

Acknowledgements

We thank Mr. Anup Kumar for his assistance in synthesizing polyaniline. This work was supported by the Department of Science and Technology, Government of India under the IRHPA scheme.

References

1 R. G. Larson, *The Structure and Rheology of Complex Fluids*, Oxford University Press, New York, 1998.
2 T. C. Halsey, *Science*, 1992, **258**, 761–766.
3 P. J. Rankin, J. M. Ginder and D. J. Klingenberg, *Curr. Opin. Colloid Interface Sci.*, 1998, **3**, 373–381.
4 W. M. Winslow, *J. Appl. Phys.*, 1949, **20**, 1137–1140.
5 H. Ma, W. Wen, W. Y. Tam and P. Sheng, *Adv. Phys.*, 2003, **52**, 343–383.
6 R. T. Bonnecaze and J. F. Brady, *J. Rheol.*, 1992, **36**, 73–115.
7 T. C. Halsey, J. E. Martin and D. Adolf, *Phys. Rev. Lett.*, 1992, **68**, 1519–1522.
8 T. C. Halsey and W. Toor, *Phys. Rev. Lett.*, 1990, **65**, 2820–2823.
9 D. J. Klingenberg and C. F. Zukoski, *Langmuir*, 1990, **6**, 15–24.

10 M. Parthasarathy and D. J. Klingenberg, *Mater. Sci. Eng., R*, 1996, **17**, 57–103.
11 H. J. Choi and M. S. Jhon, *Soft Matter*, 2009, **5**, 1562–1567.
12 J. Y. Hong and J. Jang, *Soft Matter*, 2010, **6**, 4669–4671.
13 Y. D. Liu, F. F. Fang and H. J. Choi, *Soft Matter*, 2011, **7**, 2782–2789.
14 J. Yin, X. Zhao, L. Xiang, X. Xia and Z. Zhang, *Soft Matter*, 2009, **5**, 4687–4697.
15 R. C. Kanu and M. T. Shaw, *J. Rheol.*, 1998, **42**, 657–670.
16 W. Wen, X. Huang and P. Sheng, *Soft Matter*, 2008, **4**, 200.
17 W. Wen, X. Huang, S. Yang, K. Lu and P. Sheng, *Nat. Mater.*, 2003, **2**, 727–730.
18 Y. Lan, X. Xu, S. Men and K. Lu, *Appl. Phys. Lett.*, 1998, **73**, 2908–2910.
19 H. J. Choi, M. S. Cho, J. W. Kim, C. A. Kim and M. S. Jhon, *Appl. Phys. Lett.*, 2001, **78**, 3806–3808.
20 S. G. Kim, J. Y. Lim, J. H. Sung, H. J. Choi and Y. Seo, *Polymer*, 2007, **48**, 6622–6631.
21 R. B. Bird, R. C. Armstrong and O. Hassager, *Dynamics of Polymeric Liquids, Fluid Mechanics*, Wiley-Interscience, New York, 1987.
22 M. S. Cho, H. J. Choi and M. S. Jhon, *Polymer*, 2005, **46**, 11484–11488.
23 D. Kittipoomwong, D. J. Klingenberg, Y. M. Shkel, J. F. Morris and J. C. Ulicny, *J. Rheol.*, 2008, **52**, 225–241.
24 O. Volkova, S. Cutillas and G. Bossis, *Phys. Rev. Lett.*, 1999, **82**, 233–236.
25 S. Henley and F. E. Filisko, *J. Rheol.*, 1999, **43**, 1323–1336.
26 X. Tang, W. H. Li, X. J. Wang and P. Q. Zhang, *Int. J. Mod. Phys. B*, 1999, **13**, 1806–1813.
27 K. Von Pfeil, M. D. Graham, D. J. Klingenberg and J. F. Morris, *Phys. Rev. Lett.*, 2002, **88**, 188301.
28 K. Von Pfeil, M. D. Graham, D. J. Klingenberg and J. F. Morris, *J. Appl. Phys.*, 2003, **93**, 5769–5779.
29 L. Cipelletti and L. Ramos, *J. Phys.: Condens. Matter*, 2005, **17**, R253–R285.
30 Y. M. Joshi and G. R. K. Reddy, *Phys. Rev. E: Stat., Nonlinear, Soft Matter Phys.*, 2008, **77**, 021501–021504.
31 M. Cloitre, R. Borrega and L. Leibler, *Phys. Rev. Lett.*, 2000, **85**, 4819–4822.
32 K. P. S. Parmar, Y. Méheust, B. Schjelderupsen and J. O. Fossum, *Langmuir*, 2008, **24**, 1814–1822.
33 P. Coussot, Q. D. Nguyen, H. T. Huynh and D. Bonn, *J. Rheol.*, 2002, **46**, 573–589.
34 A. Shahin and Y. M. Joshi, *Phys. Rev. Lett.*, 2011, **106**, 038302.
35 V. Awasthi and Y. M. Joshi, *Soft Matter*, 2009, **5**, 4991–4996.
36 C. J. Gow and C. F. Zukoski Iv, *J. Colloid Interface Sci.*, 1990, **136**, 175–188.
37 O. Quadrat and J. Stejskal, *J. Ind. Eng. Chem.*, 2006, **12**, 352–361.
38 J. Stejskal and R. G. Gilbert, *Pure Appl. Chem.*, 2002, **74**, 857–867.
39 H. J. Choi, T. W. Kim, M. S. Cho, S. G. Kim and M. S. Jhon, *Eur. Polym. J.*, 1997, **33**, 699–703.
40 J. U. Park, Y. S. Choi, K. S. Cho, D. H. Kim, K. H. Ahn and S. J. Lee, *Polymer*, 2006, **47**, 5145–5153.
41 T. C. B. McLeish, T. Jordan and M. T. Shaw, *J. Rheol.*, 1991, **35**, 427–448.
42 Y. M. Joshi, G. R. K. Reddy, A. L. Kulkarni, N. Kumar and R. P. Chhabra, *Proc. R. Soc. London, Ser. A*, 2008, **464**, 469–489.
43 R. Bandyopadhyay, H. Mohan and Y. M. Joshi, *Soft Matter*, 2010, **6**, 1462–1466.
44 A. S. Negi and C. O. Osuji, *Phys. Rev. E: Stat., Nonlinear, Soft Matter Phys.*, 2010, **82**, 031404.
45 P. Coussot, H. Tabuteau, X. Chateau, L. Tocquer and G. Ovarlez, *J. Rheol.*, 2006, **50**, 975–994.
46 P. Sollich, F. Lequeux, P. Hebraud and M. E. Cates, *Phys. Rev. Lett.*, 1997, **78**, 2020–2023.

